

# The effect of finger spreading on drag of the hand in human swimming

Josje van Houwelingen<sup>a,\*</sup>, Dennis H.J. Willemsen<sup>a</sup>, Rudie P.J. Kunnen<sup>a</sup>,  
GertJan F. van Heijst<sup>a</sup>, Ernst Jan Grift<sup>b</sup>, Wim Paul Breugem<sup>b</sup>, Rene Delfos<sup>b</sup>,  
Jerry Westerweel<sup>b</sup>, Herman J.H. Clercx<sup>a</sup>, Willem van de Water<sup>a,b,\*</sup>

<sup>a</sup>*Department of Applied Physics, Eindhoven University of Technology and J.M. Burgers  
Centre for Fluid Dynamics, Postbus 513, 5600 MB Eindhoven, The Netherlands.*

<sup>b</sup>*Laboratory for Aero and Hydrodynamics, Delft University of Technology and J.M. Burgers  
Centre for Fluid Dynamics, 2628 CD Delft, The Netherlands*

---

## Abstract

The effect of finger spreading on hydrodynamic drag in swimming is studied both with a numerical simulation and with laboratory experiments. Both approaches are based on the exact same 3D model of the hand with attached forearm. The virtual version of the hand with forearm was implemented in a numerical code by means of an immersed boundary method and the physical version was studied in a wind tunnel experiment. An enhancement of the drag coefficient of 2 and 5% compared to the case with closed fingers was found for the numerical simulation and experiment, respectively. A 5 and 8% favourable effect on the (dimensionless) force moment at an optimal finger spreading of 10° was found, which indicates that the difference is more outspoken in the force moment. Also an analytical model is proposed, using scaling arguments similar to the Betz actuator disk model, to explain the drag coefficient as a function of finger spacing.

*Keywords:* Human swimming, hydrodynamics, CFD, finger spreading, swimming efficiency

---

## 1. Introduction

A tantalizing question in front-crawl swimming is whether the stroke efficiency during the propulsive phase depends on spreading the fingers. Several studies exist that suggest a small increase of the drag of the hand in that case. The idea is that, although the projected area of the hand remains the same, a slight opening of the fingers still provides enough obstruction to the flow, which must be forced between the fingers. Such an increase of the drag increases

---

\*Corresponding authors

*Email addresses:* [j.v.houwelingen@tue.nl](mailto:j.v.houwelingen@tue.nl) (Josje van Houwelingen),  
[w.v.d.water@tue.nl](mailto:w.v.d.water@tue.nl) (Willem van de Water)

thrust, or gives the same thrust at lower hand velocities, both leading to enhanced swimming efficiency. For top swimmers, this may provide a competitive edge.

Since the effect is so small, its measurement or computation using numerical simulation of the flow is a challenge. Several studies exist that involve either experiments or numerical simulations, which makes a comparison between experimental and numerical results difficult. A good comparison requires a well-defined model for the hand (and forearm), combined experimental measurements and numerical computations, and clear definitions of hydrodynamic quantities to be used. For example, to quantify the drag  $F_D$ , the quantity of interest is the drag coefficient,  $C_D = F_D / \frac{1}{2} \rho A U^2$ , where  $A$  is the area of the hand projected perpendicular onto the direction of hand motion,  $\rho$  the density of the fluid and  $U$  the incoming flow velocity.

Despite differences in used models and parameter settings it is worthwhile to provide a brief overview of the main conclusions in the literature so far. Schleihauf [21] was the first to study the influence of the hand orientation and finger spacing on the hydrodynamics of swimming by conducting water channel experiments. Although marginal differences, no advantage in drag and lift coefficients for a 1.27 cm or 0.64 cm finger spread was found compared to closed fingers. Sidelnik and Young [22] performed an experiment based on an unsteady approach. A robotic arm model with closed fingers and a 10° finger spread, mimicking sculling motion, was towed through a water tank. Higher propulsive forces were obtained with spread fingers. In a numerical study, Minetti et al. [13] reported a  $C_D$  value of 0.52 and found a 8.8% drag increase compared to closed fingers for a 13° finger spacing. The size of the wake and strength of the vortices seem to determine the results [13]. The widest wake was found with optimal finger spreading. With closed fingers, larger vortices were present in the wake, while at optimal spacing the creation of such vortices was constrained by the presence of jets between the fingers. Also Marinho et al. [11] computed the  $C_D$  for three finger spreadings and found  $C_D = 1.1$  with a 5% increase of the drag coefficient for a small finger spreading compared to the case of closed fingers. They proposed that a barrier of turbulent flow is formed between the fingers. Note that the values of  $C_D$  by Minetti et al. [13] are quite different, possibly because of different sized hand and arm models (section forearm included) resulting in a different surface  $A$ . Other small discrepancies can be assigned to shape differences in hand and arm models (thumb position, definition finger spacing). Lorente et al. [9] explained the effect of finger spreading by representing the hand as an array of four cylinders. They argue that optimal spreading is the consequence of overlapping (laminar) boundary layers of individual fingers. However, the Reynolds number of their simulations is small ( $Re = 100$ ), where the effect of optimal spreading (a 28% increase) appears unrealistically large. Finally, in their steady state simulations for several orientations and hand models, Bilinauskaite et al. [2] did not find an increase of the drag force or drag coefficient when using slightly opened fingers. However, they conclude that the maximal values of local pressure for spread fingers indicate a higher pressure force and thus a higher drag force [13, 11]. Besides finger spread, a

variety of fluid dynamic aspects of swimming has recently been reviewed by Wei et al. [32] and Takagi et al. [24] while van Houwelingen et al. [27] focused on the hydrodynamics of the swimmer’s hands.

The character of the flow is quantified by the Reynolds number,  $Re = UW/\nu$ , where  $W$  is the width of the hand palm or finger, and  $\nu$  the kinematic viscosity. Taking the relative velocity of the hand with respect to the water  $U \sim 1$  m/s and the width of a finger  $\sim 0.01$  m, gives  $Re \approx 10^4$ . For a hand palm with width  $\sim 0.1$  m,  $Re$  is an order of magnitude larger. For example, the thickness of (laminar) boundary layers, denoted by  $\delta$ , around an object of size  $W$  is approximately  $\delta \propto 5Re^{-1/2}W$  [18]. With  $W = 0.01$  m, the typical boundary layer thickness around the finger is  $\delta \approx 5 \times 10^{-4}$  m. If the boundary layer is indeed of importance in describing this problem, a numerical simulation will be a challenge as a prohibitive amount of grid cells has to be used to completely resolve the flow, also in the boundary layers.

In this study we follow the unique approach where exactly the same hands were used both in numerical simulations and wind tunnel experiments, at the same value of the Reynolds number. The simulations are performed with an immersed boundary method, which is in favour for complex shaped (and moving) bodies. A similar computational technique has been used in a study on the underwater kick and different arm pull styles [31, 8], but also in the analysis of flying and swimming in nature [14], showing the tremendous potential of this approach. Five different hands were used with five different angles  $\theta$  between the fingers: the closed hand with  $\theta = 0$  and increasingly spread fingers with  $\theta = 5, 10, 15$  and  $20$  degrees (see Fig. 1 (a)), respectively. Apart from mean flow quantities, such as drag of the entire arm and the drag moment around the elbow joint, we have also studied the fluctuations in the forces. Finally, by analysing a Betz-type actuator model of the hand with variable finger spreading, for the first time a simple moment-balance explanation of the observed drag optimum is provided.

## 2. Virtual and real hands

The hands were made using the public domain software *Make Human* [10], which contains a virtual 3D model of a human, including (natural) joints. The program allowed to select the hand and arm and spread the fingers by rotating them around the joints, as is illustrated in Fig. 1(a). In combination with 3D meshing tools the hand was turned into an STL format which was used in the simulations and 3D printed for the wind tunnel. In order to study the effect of the finger spreading alone, the thumb had a fixed position. Changing the thumb abduction would have changed the projected area of the hand and would have influenced the drag and lift characteristics of the hand [21, 2, 26, 12].

The hand and forearm were digitized with  $7.5 \times 10^4$  triangular surface elements. The virtual arms, with a hand palm width, length and frontal surface of 0.59, 3.1 and 1.57, in dimensionless simulations units respectively, were used in the numerical simulations. For the wind tunnel tests the same files were used to print physical arms with 3D printing technology, with a hand palm width, length and frontal surface of 0.096 m, 0.507 m and  $0.042 \text{ m}^2$ , respectively.

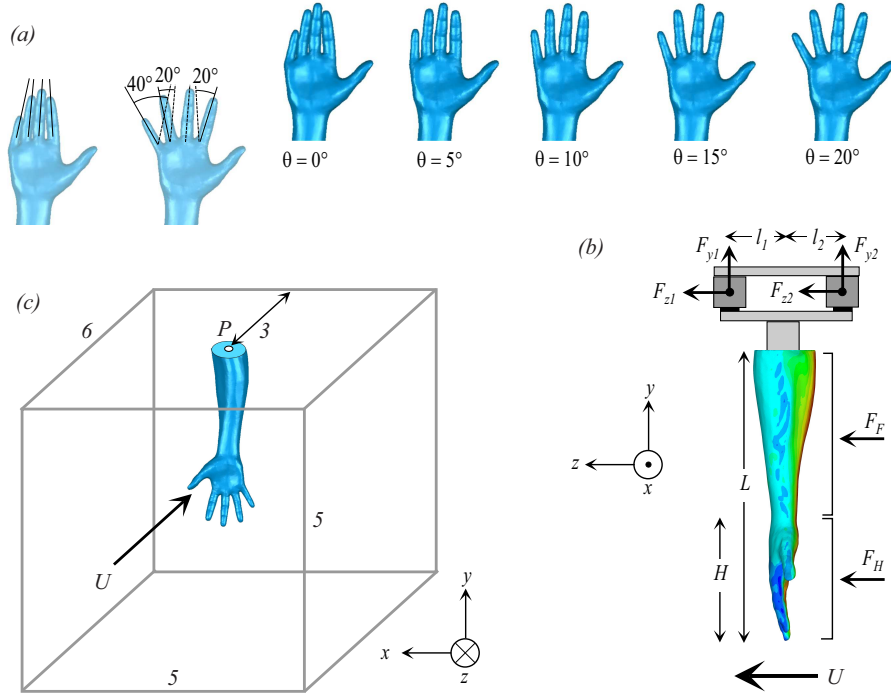


Figure 1: Panel (a) shows the five hands used. The finger spreads are 0, 5, 10, 15 and  $20^\circ$ . The angle of each finger is defined as the angle relative to the  $0^\circ$  position. For example, for the  $20^\circ$  model the index finger and ring finger are positioned  $20^\circ$  outward compared to their position in the  $0^\circ$  model, whereas the little finger is bent  $40^\circ$  outward. These angles roughly correspond to a spacing between the finger tip side edges of 0, 7.5, 15, 20 and 25 – 30 mm, respectively. Panel (b) is a schematic view of the experimental setup in the wind tunnel. Two force sensors are used in tandem configuration, which gives access to forces  $F_{x,y,z}$  and force moment  $M_x$ . The total drag force is  $F_D = F_{z1} + F_{z2}$ , the drag moment is  $M_x = l_2 F_{y2} - l_1 F_{y1}$ . The forces on the forearm and hand are  $F_F$  and  $F_H$ , respectively. Panel (c) shows the computational domain. Force moments are computed with respect to the point  $P$ .

The numerical simulations were performed using the immersed boundary method (IBM) [5]. In this IBM, the Navier-Stokes equations (NS) for an incompressible flow are solved by an integration scheme based on the fractional step method [6]. A finite difference scheme is used for discretization of the derivatives [6, 30]. IBM has the great advantage that complex boundaries can be adapted readily, without the burden of body-adapted grid generation. Therefore, IBM is very useful for the computation of flow around complex shaped, deforming and moving objects, such as swimmers. The essence is that boundaries are represented through the introduction of an extra force term in the NS equations by a direct-forcing scheme, while the grid is simply Cartesian and equidistant. Velocities are predicted on the Eulerian grid and transferred to the Lagrangian grid to be used in the direct forcing equation. This forcing is transferred back to the Eulerian grid to correct the predicted velocities [3, 5]. A moving-least-square

approximation builds the transfer functions from the Eulerian and Lagrangian grid [28].

The number of grid cells used in these simulations is  $200 \times 200 \times 240$ . The flow in the simulation is controlled through the Reynolds number  $Re$  and is set to  $10^5$  for the hand-flow configuration (based on hand palm width). At this Reynolds number the flow is turbulent. An LES (Large Eddy Simulation) solver using a Smagorinsky model is used to model the turbulent subgrid-scale stresses throughout the computational volume and to mimic the small-scale motion [19]. At the boundaries this LES approach results in an artificial boundary layer, which is much thicker than the natural one. A complete resolution of the boundary layer would have demanded  $\mathcal{O}(10^{11})$  grid cells on an equidistant mesh for our simulation setup. The alternative is a locally refined mesh, but that would have required a much more complex code. However, at current hand speeds the boundary layer at the fingers is thin,  $\delta \approx 5 \times 10^{-4}$  m. This suggests that the boundary layer is not increasing the effective frontal area of the hand significantly and is thus of minor importance in describing enhanced drag in the finger spacing problem.

The numerical method was tested on the flow around circular cylinders and around a sphere, which are very well documented [15]. The value of the drag coefficient  $C_D$  as a function of the Reynolds number was reproduced to within 10% for  $10^3 \lesssim Re \lesssim 10^5$ , and so was the dimensionless vortex shedding frequency for the cylinder, denoted by the Strouhal number  $Sr = fD/U = 0.23 \pm 0.01$ , with  $D$  the diameter of the cylinder and  $f$  the measured frequency. As expected, the drag crisis around  $Re \approx 3 \times 10^5$ , where the upstream boundary layer turns turbulent, is missed in these simulations due to a lack of resolution and the used turbulence model near the surface of the body. However, it should be noted that this value of  $Re$  is not reached in the simulations of the hand, in particular not around the fingers.

The computational domain, shown schematically in Fig. 1(c), is a cuboid with size  $5 \times 5 \times 6$ . The origin is located on the inlet at the center of the XY-plane. Uniform inflow with velocity  $U = 1$  was specified on the plane  $z = 0.0$ , whereas radiative outflow conditions  $\partial \mathbf{u} / \partial z = \mathbf{0}$  were used at  $z = 6.0$ . Stress-free boundary conditions were imposed at  $y = \pm 2.5$  and no-slip conditions on the body, and periodic boundaries were taken at  $x = \pm 2.5$ . Point  $P$  (see Fig. 1c) of the  $L = 3.096$  long arm was located at  $(x, y, z) = (0, 2.5, 3.0)$ , which allowed a wake of 3 length units to develop.

The wind tunnel experiments were carried out in the 8 m long and  $1.1 \times 0.7$  m<sup>2</sup> test section of a recirculation wind tunnel at the TU/e Fluid Dynamics Laboratory. The arm was mounted on two connected force sensors so that all three components of the total force and one component  $M_x = l_2 F_{y_2} - l_1 F_{y_1}$  of the torque could be measured. A schematic view of the setup is shown in Fig. 1(b). To give an idea of the typical magnitude of forces and their fluctuations: at a largest mean wind velocity  $U = 15.4$  m/s, and a finger spreading of  $20^\circ$ , the typical mean force measured is  $F_z = 6.6$  N, with root-mean-square (rms) fluctuation  $\delta F_z = 0.3$  N. For this case the Reynolds number is  $Re = 1.03 \times 10^5$ . Due to the finite stiffness of the setup mechanical vibrations thwarted the measurement

of fluctuations due to vortex shedding and turbulence. Still, this measurement of the drag was preferred over one involving the integration of measured pressures over the hand surface as its complex geometry would have called for a prohibitive number of pressure taps. The forearm of the model, together with the suspension and the force sensors partly sit in the wind tunnel boundary layer (with a typical thickness of approximately 0.15 m), so that the approaching flow over the model is not entirely uniform. Therefore, the measured torque, which is biased towards forces on the hand, provides a better comparison between experiment and simulations.

The quantities of interest in both simulations and experiments are the total forces  $F_x, F_z$  on the arm and the torque  $M_x$  with respect to the point  $P$  at the end of the forearm. The torque  $M_x$  is interesting as it is biased towards the forces exerted on the hand and is determined to a lesser extent by the proximal part of the arm. Accordingly, we define drag, lift and drag-moment coefficients as

$$C_{D,L} = \frac{F_{z,x}}{\frac{1}{2}\rho AU^2}, \quad \text{and} \quad C_{M_x} = \frac{M_x}{\frac{1}{2}\rho ALU^2},$$

respectively, where  $A$  is the projected area of the hand and arm perpendicular onto the direction of uniform inflow, and  $L$  its length. In simulation units,  $A = 1.574$  and  $L = 3.096$ , which have to be scaled accordingly for the physical arms (which have a length of 0.516 m).

The measurement of both drag and drag moment allows for a crude distinction between the drag force  $F_F$  experienced by the forearm and the drag force  $F_H$  experienced by the hand,

$$|M_x| = \frac{1}{2}(L - H)\tilde{F}_F + (L - H/2)\tilde{F}_H,$$

where  $H$  is the length of the hand,  $H \sim 1.2$  in simulation units,  $L$  is the length of the complete hand-arm model,  $L = 3.1$ , and  $\tilde{F}_F$  and  $\tilde{F}_H$  are the moment-averaged forces on the arm and hand respectively,

$$\begin{aligned} \tilde{F}_F &= \frac{2}{L - H} \int_0^{L-H} y \delta F_z(y) dy, \quad \text{and} \\ \tilde{F}_H &= \frac{1}{L - H/2} \int_{L-H}^L y \delta F_z(y) dy, \end{aligned} \quad (1)$$

with  $\delta F_z(y) dy$  the force in the flow direction on a slice with infinitesimal width  $dy$ . For convenience,  $\tilde{F}_F$  is approximated by the total force  $F_F = \int_0^{L-H} \delta F_z(y) dy$ , which is valid when the force across the arm is constant. A similar reasoning holds for  $F_H$ . Then

$$\begin{aligned} F_H &= \frac{2}{L}|M_x| - (1 - H/L)F_{\text{tot}}, \quad \text{and} \\ F_F &= -\frac{2}{L}|M_x| + (2 - H/L)F_{\text{tot}}, \end{aligned} \quad (2)$$

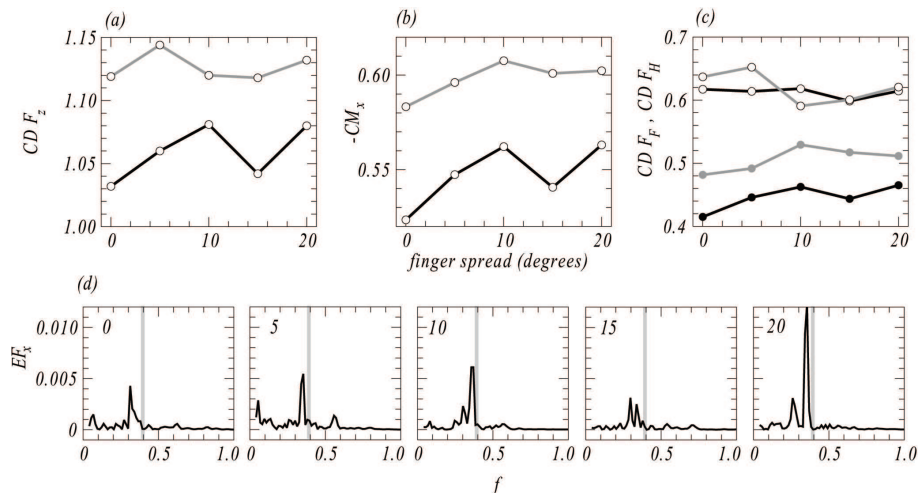


Figure 2: Panels (a, b, c) show the drag coefficient  $C_D$ , the drag moment coefficient  $C_{M_x}$  (note the minus sign) and the normalized dimensionless forces on the forearm (open symbols) and the hand (closed symbols). These forces are defined in Eq. 2. Symbols connected by black lines are numerical simulations, gray lines are the experimental results. Energy spectra of the dimensionless cross (lift) force  $C_L$  are shown in (d) for the 5 finger spreadings used. The vertical grey lines indicate the computed shedding frequency of the hand and fingers, assuming a Strouhal number  $Sr = 0.23$ .

where  $F_{tot} = F_F + F_H$  is the total measured force. These are useful quantities as they can be measured both in the numerical simulation and in the wind tunnel experiments.

Both experiments and immersed boundary simulations produced time series of the force components  $F_{x,y,z}(t)$  and the torque  $M_x(t)$ , which allowed the computation of fluctuations. These were quantified by their power spectra  $E_{F_{x,y,z}}(f), E_{M_x}(f)$ . Averaged power spectra were computed using Fourier transforms over half overlapping time windows with length  $T = 73$  (simulations units), while a filter  $\sin^2(\pi t/T)$  reduced spectral leakage. Since the averages were done over long times series, the statistical error of mean quantities is negligible. The only inaccuracies are caused by systematic errors in the setup and method.

### 3. Results

Results of the experiments and the numerical simulations are shown in Fig. 2. The simulations predict an increase of total force and torque for every spacing larger than  $0^\circ$ , with local maxima around  $10^\circ$  and  $20^\circ$ . The experiments show a similar increase for the torque, but just local maxima for the force at  $5^\circ$  and  $20^\circ$ . The enhancement for the first local maximum compared to the hand with closed fingers is small, being 2% and 5% for the experiment and numerical simulation, respectively. The absolute values of drag and torque differ by 10%

between experiment and simulation. Most relevant for this study, however, is the *variation* of the drag and torque with finger spreading.

As forces on the hand have a larger weight in the evaluation of the dimensionless force moment  $C_{M_x}$ , the effect of optimal finger spreading is larger here, 5% and 8% for the experiment and numerical simulation, respectively. Also, the found optimal finger spreading of  $10^\circ$  is the same in experiment and numerical simulation. The difference between the numerical and experimental results is probably due to the non-uniform flow profile on the forearm in the wind tunnel and possibly unsolved flow properties in the simulations. The second local maximum might suggest different wake structures, like the flow around a cylinder pair [23], but should be further investigated.

Fig. 2 also shows the (approximate) division of the forces over forearm ( $F_F$ ) and hand ( $F_H$ ) (see Eq. 2) in the numerical simulations and experiments. As expected, the force on the forearm remains approximately constant, while that on the hand increases with increasing finger spreading. Depending on the execution of the front-crawl stroke an additional effect should be taken into account. The relative velocity of the hand is (much) larger than that of the forearm, so that the influence of finger spreading also becomes larger.

The energy spectra of the dimensionless side (lift) force  $C_L$  show a peak at a dimensionless frequencies  $f = 0.31 - 0.36$ . This coherent force fluctuation is due to vortex shedding. Taking the diameter of the forearm 0.60 and a Strouhal number  $Sr = 0.23$ , which is characteristic for vortex shedding off a cylinder [15], the calculations predict a frequency  $f = 0.38$ , which agrees well with the observed frequency. Vortex shedding reaches a local maximum at the optimal finger spreading, decreases at  $\theta = 15^\circ$ , and is strongest at  $\theta = 20^\circ$ . Both experiments and simulation show a drag minimum at  $15^\circ$ , after which the drag rises again for the fingers spread uncomfortably at  $20^\circ$ . The same behavior can be observed in the vortex shedding. It is believed that this is due to interaction between the flow around the arm and the fingers.

#### 4. Actuator disk model

The drag optimum of a hand with spread fingers can be described using the actuator disk concept, which elegantly predicts the maximum efficiency of a wind turbine [1]. The idea there is to replace the wind turbine by a disk and compute the power that passes through the disk using Bernoulli and conservation of mass and momentum. Inspired by this concept, the four fingers with width  $D$  and gaps with width  $d$  are modelled as an actuator disk (see Fig. 3). A scaling description of the effect of finger spreading is obtained by modelling the flow in between the fingers as a pressure driven channel flow.

Briefly, let the control volume of mass- and momentum conservation be determined by the size of the actuator disk with area  $A = L(4D + 3d)$ . Let  $V_1$  be the velocity entering the control volume and  $V_2$  the mean velocity leaving the volume behind the actuator disk. Now assume, that stream tube deflection happens before the actuator disk and has a constant width behind the disk. Therefore, the mean velocity through the actuator disk  $V_d$  can be approximated by  $V_2$  and



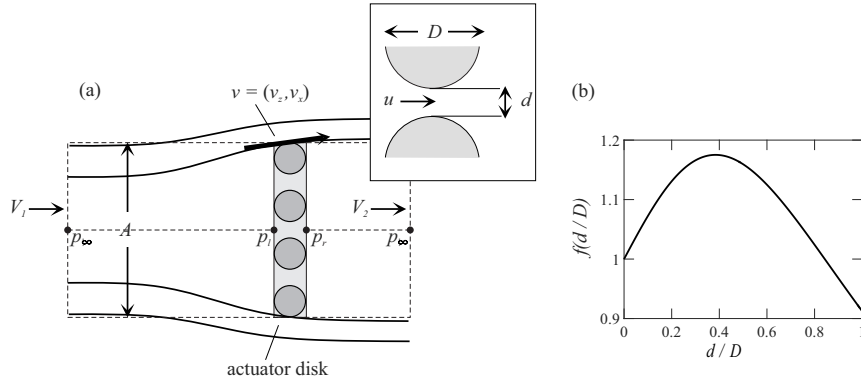


Figure 3: Panel (a) illustrates how to represent the hand as an “actuator disk”, an effective surface of area  $A$  that causes the drag. This actuator disk is shown greyed. The inset illustrates the flow  $u$  that in between the fingers, driven by a pressure difference  $\Delta p$  across the hand,  $u^2 = \xi \Delta p d / (\rho D)$ , with friction factor  $\xi$ . The resulting normalized drag  $f(d/D)$  is shown in panel (b).

$p_r \approx p_\infty$  (see Fig. 3). Conservation of mass leaves us with an average vertical velocity  $\tilde{v}_x = \frac{1}{2}(V_1 - V_2)$  at the top and bottom surfaces of the control volume, which will be used in conservation of momentum. The change in horizontal velocity from  $V_1$  towards  $V_2$  happens before the disk, the horizontal velocity  $v_z$  can be locally approximated with the average  $\frac{1}{2}(V_1 + V_2)$ . Using this, conservation of momentum gives an expression for the drag force  $F_D = \frac{1}{2}\rho A(V_1^2 - V_2^2)$ . The pressure difference across the disk,  $\Delta p = \frac{1}{2}\rho(V_1^2 - V_2^2)$ , can be obtained with Bernoulli. Now assume, similarly to fluid flow through a channel with width  $d$  and length  $D$  [17], that the velocity  $u$  of the water forced between the fingers follows from the pressure difference  $\Delta p$  over the disk as  $u^2 = \xi \Delta p d / (\rho D)$ , with a friction factor  $\xi$ . Imposing mass balance,  $A V_2 = 3L du$ , results in an expression for the unknown velocity  $V_2$ .

The difference with the original Betz argument is the change of geometry of the stream tube as fingers are spread. As a function of the dimensionless finger spreading  $\alpha = d/D$  the change of the drag, relative to that of the closed hand, is

$$f_D = \frac{1}{2}\rho V_1^2 4DL (1 + 3\alpha/4) (1 + \beta)^{-1} = \frac{1}{2}\rho V_1^2 4DL f(\alpha), \quad (3)$$

with  $\beta = (9/2)\xi\alpha^3/(4 + 3\alpha)^2$ . The function  $f(\alpha)$  is such that  $f(0) = 1$ . It is plotted in Fig. 3(b) for  $\xi = 10$ , which is realistic value. It shows an optimum drag enhancement of  $\sim 17.5\%$  for a small finger spreading  $\alpha = 0.38$ . It is not very surprising that this simple argument qualitatively predicts the drag optimum for a small finger spreading, as it embodies the notion that the effective area of the hand is increased by spreading the fingers because a small opening of the fingers still presents an obstruction of the flow between them. Thus, the effective area of the spread hand increases until the gap between the fingers becomes so large that it no longer resists the flow. Since the model is only for the four fingers,

the enhancement of the drag for the arm-hand combination is approximately one quarter of this value. It is remarkable that this approximately agrees with enhancement in force measured in the experiment and simulation.

## 5. Conclusion

We conclude that immersed boundary methods, which were first applied to swimming by Loebbecke and Mittal [8], provide a viable tool for understanding also the fine details of swimming, such as finger spreading. The strength of IBM is its accommodation of complex deforming boundaries at low computational costs. We also emphasize the usefulness of force moments which most clearly show the influence of finger spreading. We finally stress the importance of flow-induced force (moment) fluctuations. We find a positive correlation between the magnitude of periodic vortex shedding and drag, while others may have found an adverse effect [13]. Coherent fluid motion in the form of vortices is an example of flow structures influencing swimming efficiency. Future research will focus on these structures. A scaling argument, similar to the Betz actuator disk model [1], predicts the observed drag optimum. Swimming propulsion necessarily comes with drag. An increase of the drag of the hand by spreading fingers reduces the slip velocity between the hand and the water and diminishes the power dissipated for propulsion. This increases swimming efficiency. The effect is, however, quite small, but may provide a competitive edge.

The significance of optimal finger spreading can be roughly quantified in terms of swimming time. A swimmer can reach a speed of  $v_s = 2$  m/s in front crawl swimming and experiences a drag force of  $F_D = 100$  N [25, 33, 29, 16]. Assume that the stroke frequency of a complete cycle is  $0.5$  s<sup>-1</sup> (propulsive phase of one arm takes 1 s) and the backward (slip) velocity of the hand with respect to the water is  $v_h = 2.2$  m/s [2, 20, 7, 4]. Furthermore, assume that the projected area of the hand is  $0.042$  m<sup>2</sup> and that the drag coefficient  $C_D = 1.03$ . This yields a propulsive force produced by the hand and arm of  $F_h = 105$  N. The swimmer needs more than  $200$  W power to overcome drag ( $P_D = F_D v_s$ ). The power produced by just the hands and forearms is  $P_h = F_h v_h = 230$  W (human swimming is inefficient). The (mechanical) power of the swimmer is given by  $P_s = P_D + P_h$ , with a power loss to overcome drag  $P_D$  due to the motion of the complete body and a power loss due to the movement of the limbs  $P_h$  for generating propulsion. Practically, the swimmer will yield the same power  $P_s$ , supplied muscle force ( $F_h$  for the hand) and drag force  $F_D$  when changing to a new technique. When obtaining an optimal finger spreading,  $C_D$  can increase upto  $1.08$ . This allows a decrease of  $v_h$  and  $P_h$ , since  $F_h$  is fixed. The reduction of the power loss at the hand of  $5$  W can be used in favour of overcoming the drag  $P_D$ , resulting in a  $2.5\%$  velocity increase of the swimmer  $v_s = P_D/F_D$ . This equals an improvement of one's personal best of  $0.6$  s on the  $50$  m freestyle. This result might be slightly exaggerated. An unsteady approach would give a more underpinned answer, as the present approach only applies to a snapshot of the stroke. However, looking back at the women's  $50$  m freestyle final at the Rio 2016 Summer Olympics, where the first up to sixth place were decided within

0.12 s, a marginal change in technique indeed could be the difference between a gold medal and no medal at all.

### **Conflict of Interest**

The authors declare that they have no conflict of interest.

### **Acknowledgment**

This project was supported by the STW (‘Stichting Technische Wetenschappen’) research program Sport (project #12868). The authors hereby express their gratitude to Roberto Verzicco for making available the IBM code and for help in implementing it.

### **References**

#### **References**

- [1] Betz, A., 1966. Introduction to the Theory of Flow Machines. Oxford: Pergamon Press.
- [2] Bilinauskaite, M., Mantha, V., Rouboa, A., Ziliukas, P., Silva, A., 2013. Computational fluid dynamics study of swimmer’s hand velocity, orientation, and shape: Contributions to hydrodynamics. *J. BioMed. Res. Int.* 1, 140487.
- [3] Fadlun, E., Verzicco, R., Orlandi, P., Mohd-Yusof, J., 2000. Combined immersed-boundary finite-difference methods for three-dimensional complex flow simulations. *J. Comput. Phys.* 161, 35–60.
- [4] Gourgoulis, V., Boli, A., Aggelousis, N., Antoniou, P., Mavromatis, G., 2014. The influence of the hand’s acceleration and the relative contributions of drag and lift forces in front crawl swimming. *J. Sports Sci.* 33, 696–712.
- [5] Iaccarino, G., Verzicco, R., 2003. Immersed boundary technique for turbulent flow simulations. *Appl. Mech. Rev.* 56 (3), 331–347.
- [6] Kim, J., Moin, P., 1985. Application of a fractional step method to incompressible navier-stokes equations. *J. Comput. Phys.* 59, 308–323.
- [7] Kudo, S., Vennell, R., Wilson, B., 2013. The effect of unsteady flow due to acceleration on hydrodynamic forces acting on the hand in swimming. *J. Biomech.* 46, 1697–704.
- [8] Loebbecke, A., Mittal, R., 2012. Comparative analysis of thrust production for distinct arm-pull styles in competitive swimming. *J. Biomech. Eng.* 134, 074501.

- [9] Lorente, S., Cetkin, E., Bello-Ochende, T., Meyer, J., Bejan, A., 2012. The constructal-law physics of why swimmers must spread their fingers and toes. *J. Theor. Biol.* 308, 141–146.
- [10] MakeHuman-Team, 2001–2016. Makehuman.  
URL [www.makehuman.org](http://www.makehuman.org)
- [11] Marinho, D., Barbosa, T., Reis, V., Kjendlie, P., Alves, F., Vilas-Boas, J., Machado, L., Silva, A., Rouboa, A., 2010. Swimming propulsion forces are enhanced by a small finger spread. *J. Appl. Biomech.* 26, 87–92.
- [12] Marinho, D., Rouboa, A., Alves, F., Vilas-Boas, J., Machado, L., Reis, V., Silva, A., 2009. Hydrodynamic analysis of different thumb positions in swimming. *J. Sports Sci. Med.* 8, 58–66.
- [13] Minetti, A., Machtsiras, G., Masters, J., 2009. The optimum finger spacing in human swimming. *J. Biomech.* 42 (13), 2188–2190.
- [14] Mittal, R., Dong, H., Bozkurttas, M., Von Loebbecke, A., Najjar, F., 2006. Analysis of flying and swimming in nature using an immersed boundary method. In: 36th AIAA Fluid Dynamics Conference and Exhibit: San Francisco, California, 5-8 June 2006: conference proceedings. Vol. 51. p. 6180.
- [15] Munson, B., Young, D., Okiishi, T., Huebsch, W., 2009. *Fundamental of Fluid Mechanics*, 6th Edition. John Wiley & Sons, Inc.
- [16] Novais, M., Silva, A., Mantha, V., Ramos, R., Rouboa, A., Vilas-Boas, J., Luis, S., Marinho, D., 2012. The effect of depth on drag during the streamlined glide: a three-dimensional cfd analysis. *J. Hum. Kinet.* 33, 55–62.
- [17] Pope, S., 2000. *Turbulent Flows*. Cambridge, 292.
- [18] Prandtl, L., 1956. *Strömungslehre*. Braunschweig: Friedr. Vieweg & Sohn.
- [19] Sagaut, P., 2006. *Large Eddy Simulation for Incompressible Flows: an Introduction*, 2nd Edition. Springer-Verslag.
- [20] Sato, Y., Hino, T., 2001. Estimation of thrust of swimmer’s hand using cfd. In: 2nd International Symposium on Aqua Bio-Mechanisms. Hawaii, p. 1.
- [21] Schleihauf, R., 1979. Hydrodynamic analysis of swimming. In: *Third International Symposium on Biomechanics in Swimming*. Edmonton, Canada, pp. 70–109.
- [22] Sidelnik, N. O., Young, B. W., 2006. Optimising the freestyle swimming stroke: the effect of finger spread. *Sports Eng.* 9 (3), 129–135.
- [23] Sumner, D., 2010. Two circular cylinders in cross-flow: a review. *J. Fluids Struct* 26, 849–899.

- [24] Takagi, H., Nakashima, M., Sato, Y., Matsuuchi, K., Sanders, R., 2016. Numerical and experimental investigations of human swimming motions. *J. Sport. Sci.* 34 (16), 1564–1580.
- [25] Takagi, H., Shimizu, Y., Kodan, N., 1999. A hydrodynamic study of active drag in swimming. *JSME Int. J. B.* 42, 2.
- [26] Takagi, H., Shimizu, Y., Kurashima, A., Sanders, R., 2001. Effect of thumb abduction and adduction on hydrodynamic characteristics of a model of the human hand. In: *Proceedings of swim sessions of the XIX international symposium on biomechanics in sports*. University of San Francisco, pp. 122–126.
- [27] van Houwelingen, J., Schreven, S., Smeets, J., Clercx, H., Beek, P., 2016. Effective propulsion in swimming: Grasping the hydrodynamics of hand movements. *J. Appl. Biomech.* In press.
- [28] Vanella, M., Balaras, E., 2009. A moving-least-square reconstruction for embedded boundary formulation. *J. Comput. Phys.* 228 (18), 6617–6628.
- [29] Venell, R., Pease, D., Wilson, B., 2006. Wave drag on human swimmers. *J. Biomech.* 39, 664–671.
- [30] Verzicco, R., Orlandi, P., 1996. A finite-difference scheme for three-dimensional incompressible flows in cylindrical coordinates. *J. Comput. Phys.* 123 (2), 402–414.
- [31] von Loebbecke, A., Mittal, R., Fish, F., Mark, R., 2009. Propulsive efficiency of the underwater dolphin kick in humans. *J. Biomech. Eng.* 131, 054504.
- [32] Wei, T., Mark, R., Hutchison, S., 2014. The fluid dynamics of competitive swimming. *Annu. Rev. Fluid Mech.* 46, 547–565.
- [33] Zamparo, P., Gatta, G., Pendergast, D., Capelli, C., 2009. Active and passive drag: the role of trunk incline. *Eur. J. Appl. Physiol.* 106, 195–205.